

Electronic Supplementary Information

Dual Strategy of Molecular-Weight Control and Ionic Doping in Poly(benzodifurandione) for Energy-Efficient Neuromorphic OECTs

José Carlos Pérez Martínez,¹ Ignacio Sanjuán*,¹ David Franco,¹ Isaac Sánchez-Márquez,¹ Baurzhan Ilyassov,² Qun-Gao Chen,³ Wen-Ya Lee,³ Chu-Chen Chueh,⁴ and Antonio Guerrero*¹

¹ Institute of Advanced Materials (INAM), Universitat Jaume I, 12006 Castelló, Spain.

² Astana IT University, Mangilik El avenue 55/11, Business center EXPO, block C1, Astana, 010000, Kazakhstan

³ Department of Chemical Engineering and Biotechnology, National Taipei University of Technology, Taipei 106344, Taiwan

⁴ Department of Chemical Engineering, National Taiwan University, Taipei 10617, Taiwan

Corresponding authors: I Sanjuán (i.sanjuan@uji.es), A. Guerrero (aguerrer@uji.es)

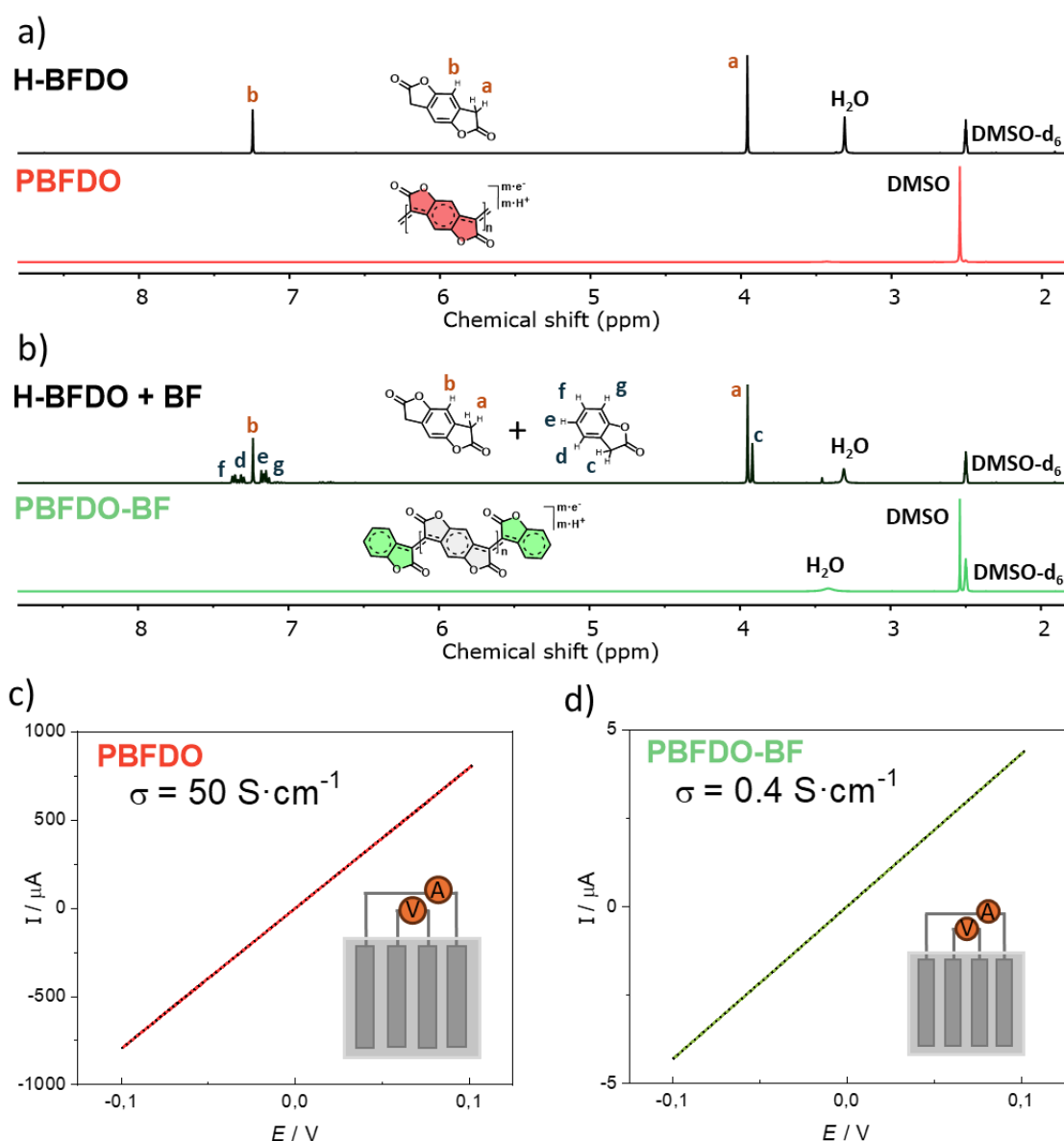


Figure S11. Characterization of the synthesized polymers by ¹H-RMN and I-V voltammetry. a) ¹H-RMN spectra of the monomer H-BFDO (top) and the PBFDO after polymerization (bottom). b) ¹H-RMN spectra of the mixture monomer H-BFDO + end-capper BF (top) and the PBFDO-OH after polymerization (bottom). c - d) I-V measurements to measure the electrical conductivity of spun-coated films of (c) PBFDO and (d) PBFDO-OH using the four-probe technique.

The absence of signals in the ¹H-RMN spectra confirms the full conversion of the monomer BDF and the end capper BF to yield the PBFDO and PBFDO-BF, respectively. The lack of ¹H-NMR resonances can be attributed to its conjugated backbone and paramagnetic signal broadening arising from its doping. The two orders of magnitude lower electrical conductivity of the PBFDO-BF compared to the PBFDO can be explained by a shorter polymer chain length.

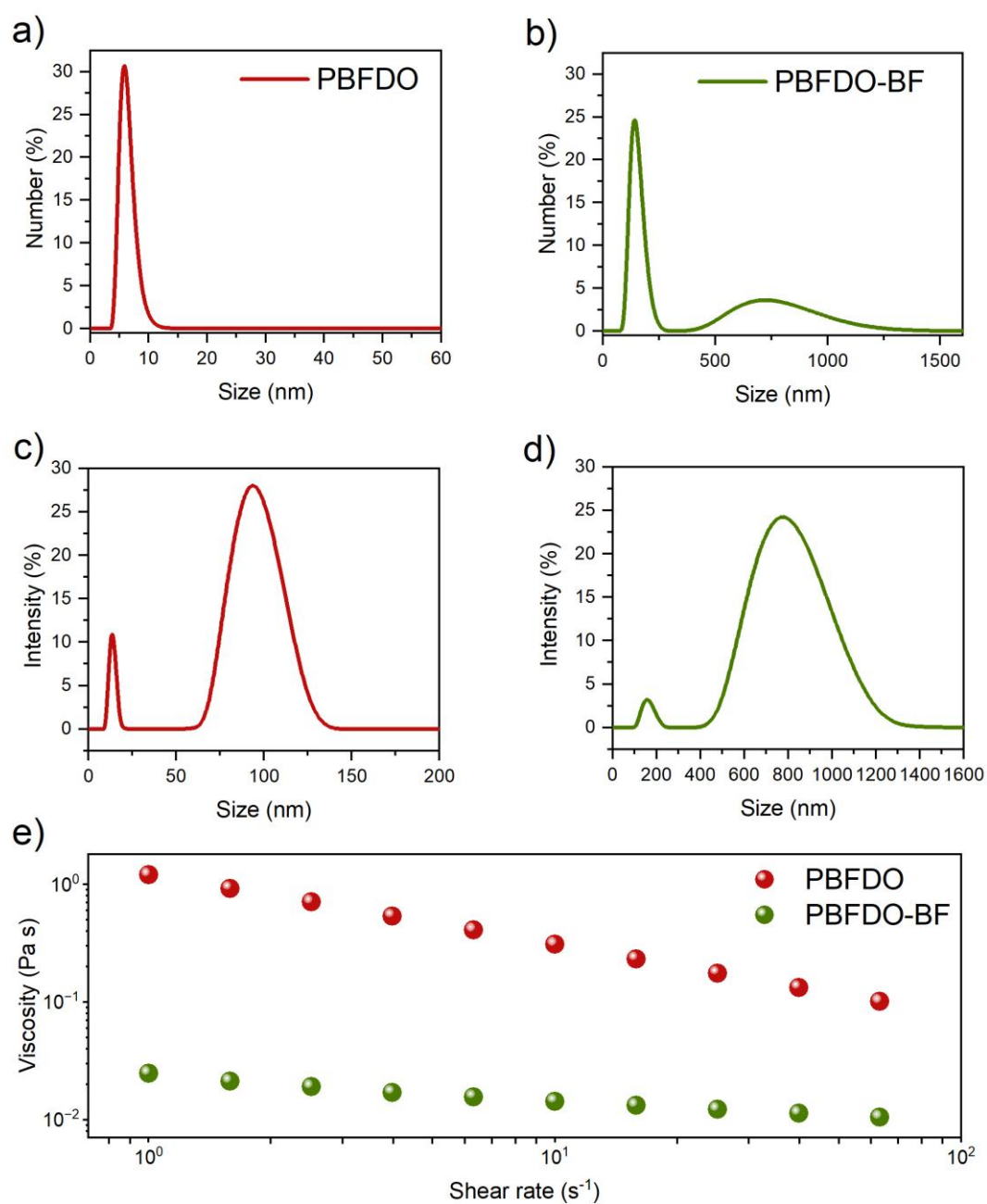


Figure SI2. (a-d) Dynamic Light Scattering (DLS) measurements for the PBFDO (a, c) and the PBFDO-BF (b, d). e) Rheological analysis of the viscosity of both polymers.

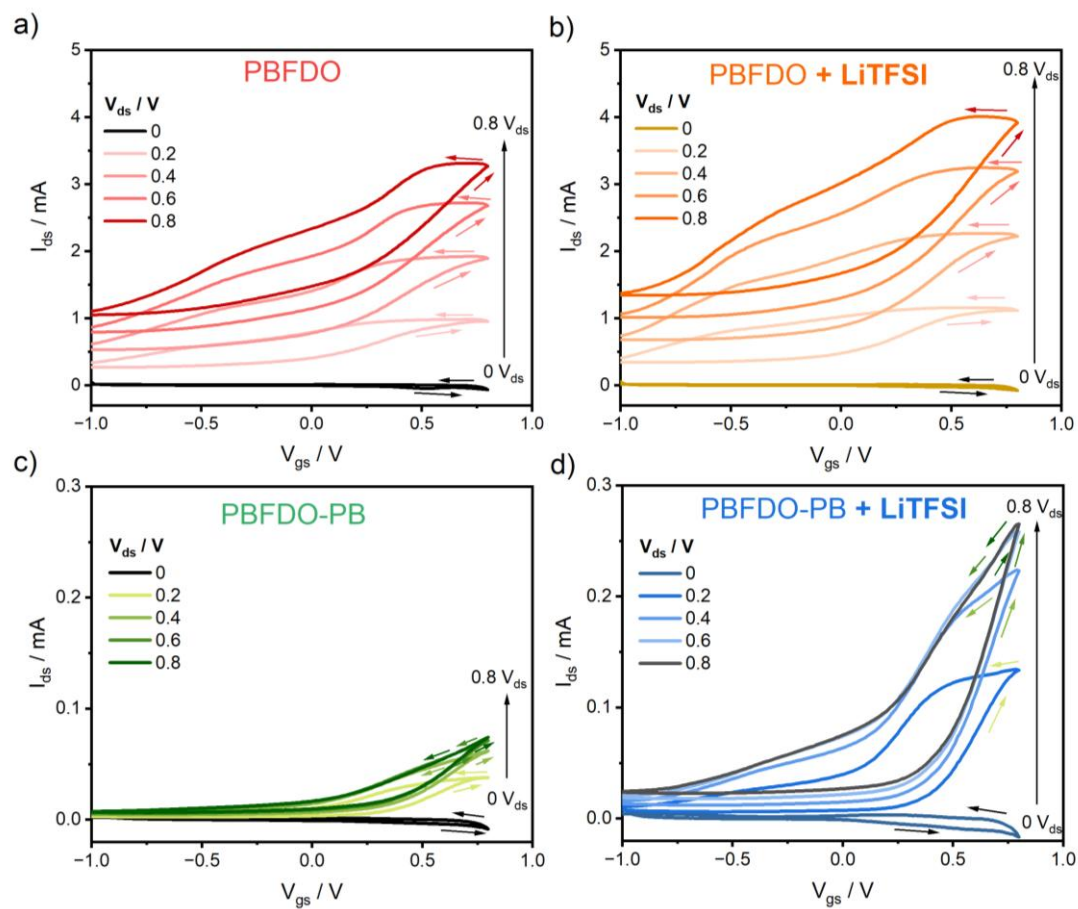


Figure SI3. Transfer characteristic curves for the OEFTs fabricated with a) PBFDO, b) PBFDO + LiTFSI 5 wt.%, c) PBFDO-PB, d) PBFDO-PB + LiTFSI 5 wt.%. Scan rate: 30 mV s^{-1} .

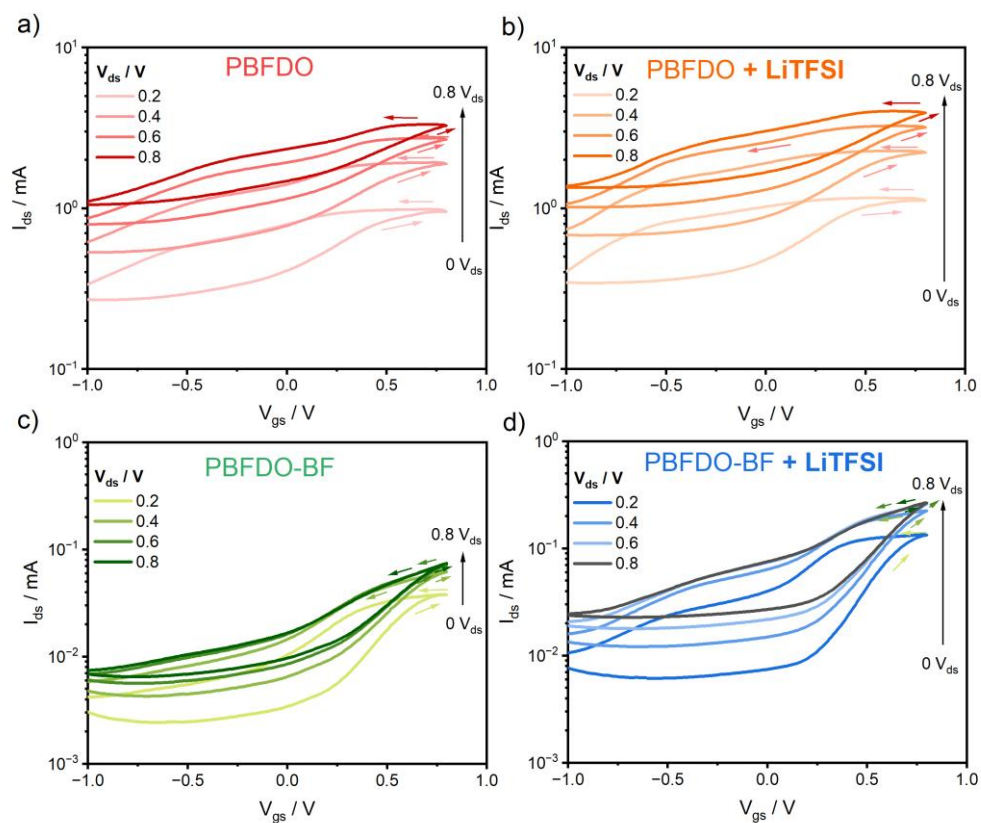


Figure SI4. Transfer characteristic curves in semilogarithmic scale for the OEFTs fabricated with a) PBFDO, b) PBFDO + LiTFSI 5 wt.%, c) PBFDO-BF, d) PBFDO-BF + LiTFSI 5 wt.%. Scan rate: 30 mV s⁻¹.

Spiking-Width-Dependent Plasticity (SWDP)

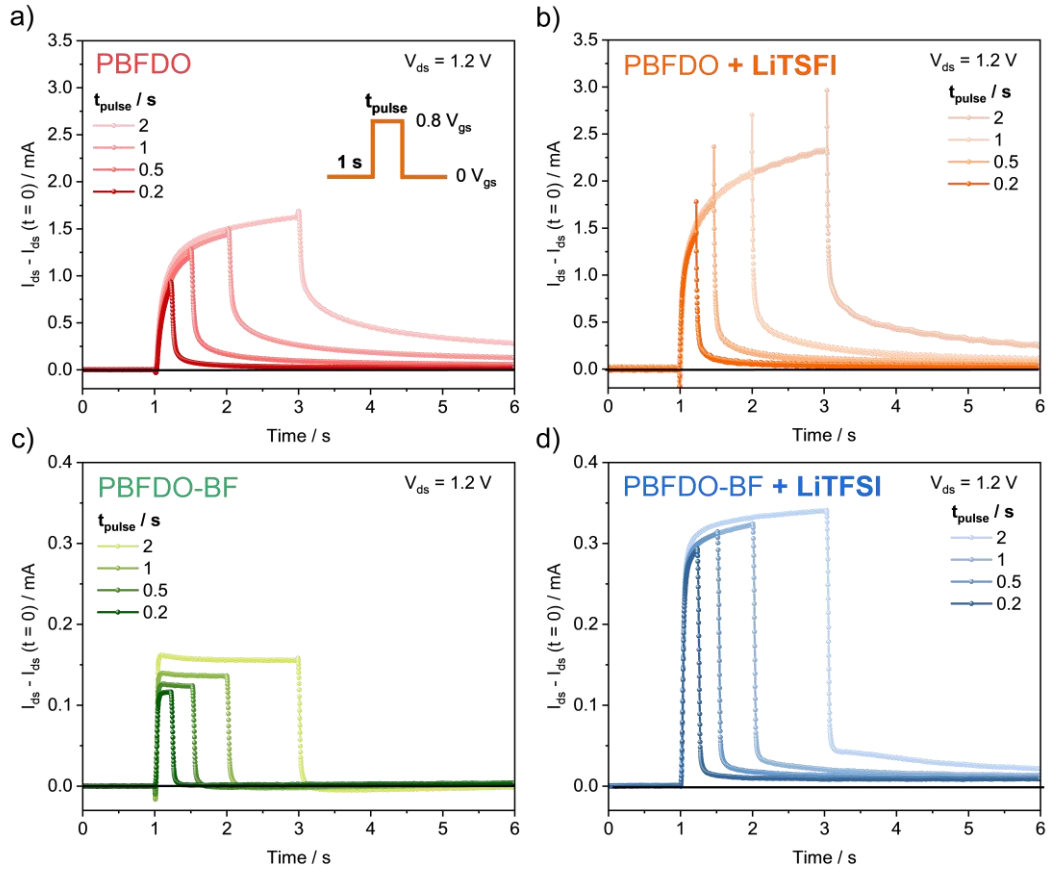


Figure S15. Transient drain current response upon the application of gate voltage pulses of different widths, for OEFTs fabricated with a) PBFDO, b) PBFDO + LiTFSI, c) PBFDO-BF, and d) PBFDO-BF + LiTFSI. Parameters: $V_{gs}(\text{pulse}) = 0.8 \text{ V}$, $V_{gs}(\text{read}) = 0 \text{ V}$, $V_{ds} = 1.2 \text{ V}$. The devices are deactivated to the OFF state before the pulse by applying $V_{gs} = -0.8 \text{ V}$ for 20 s. Drain currents are subtracted with the drain currents at $t = 0$.

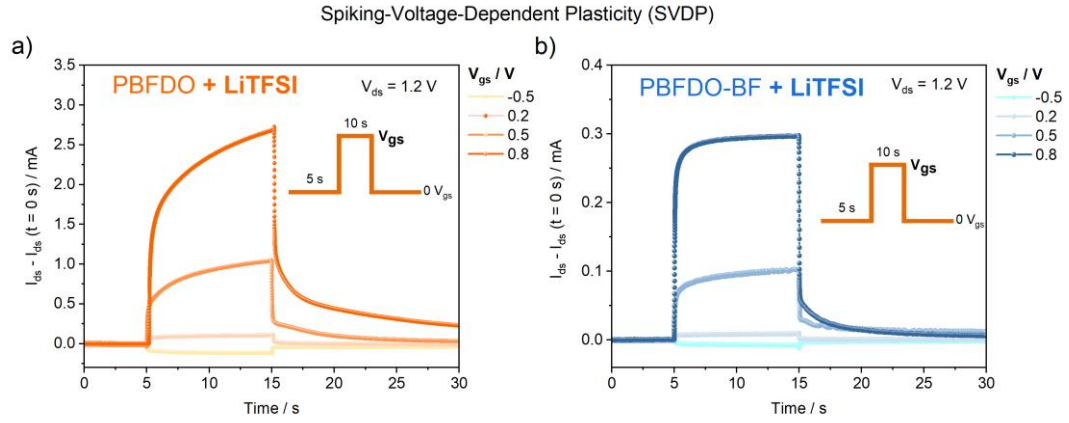


Figure SI6. Transient drain current response upon the application of gate voltage pulses of different voltages, for OECTs fabricated with a) PBFDO + LiTFSI, and b) PBFDO-BF + LiTFSI. Parameters: Pulse width = 10 s, V_{gs} (read) = 0 V, $V_{ds} = 1.2$ V. Drain currents are subtracted with the drain currents at $t = 0$.

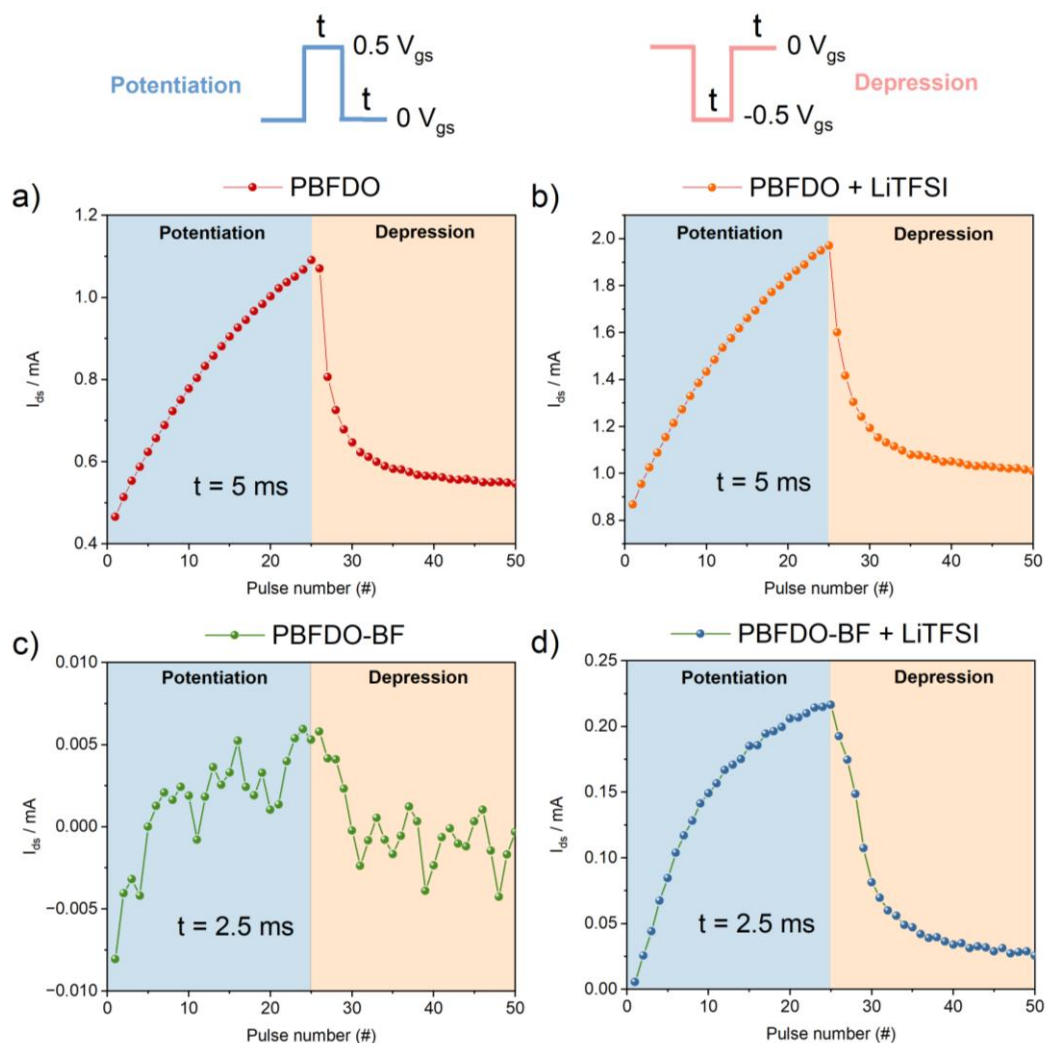


Figure SI7. Long-term potentiation (LTP) and long-term depression (LTD) cycles for the a) PBFDO OECTs, b) PBFDO + LiTFSI OECTs, c) PBFDO-BF OECTs, and d) PBFDO-BF + LiTFSI OECTs. Each LTP/LTD cycle is built upon the application of 25 consecutive pulses at $V_{gs} = 0.5 \text{ V}$ (set voltage) followed by 25 pulses at $V_{gs} = -0.5 \text{ V}$ (reset voltage). $V_{gs}(\text{read}) = 0 \text{ V}$, $t_{\text{pulse}} =$ (a, b) 5 ms, (c, d) 2.5 ms.